HHS Public Access

Author manuscript

Macromolecules. Author manuscript; available in PMC 2024 January 18.

Published in final edited form as:

Macromolecules. 2023 November 14; 56(21): 8565–8573. doi:10.1021/acs.macromol.3c01400.

Network Constitutional Isomers

Brandon R. Clarke,

Department of Polymer Science and Engineering, University of Massachusetts Amherst, Amherst, Massachusetts 01003, United States;

Gregory N. Tew

Department of Polymer Science and Engineering, University of Massachusetts Amherst, Amherst, Massachusetts 01003, United States;

Abstract

Bottlebrush networks designed to be constitutional isomers of each other were synthesized for the first time. These network constitutional isomers (NCIs) have significantly different mechanical properties depending on their kinetic chain lengths (R_K), which are controlled by the monomer-to-initiator ratio. Specifically, the low frequency moduli, yield behavior, elongation at break, and adhesive strength of these NCIs are different at the same cross-link densities. The NCI concept is extended to include R_Ks' dispersity through the choice of the catalyst. These NCIs highlight the impact of living polymerization chemistry on network formation. The use of living polymerization chemistry to synthesize new networks, including NCIs, is expected to significantly advance the development of next-generation materials.

Graphical Abstract

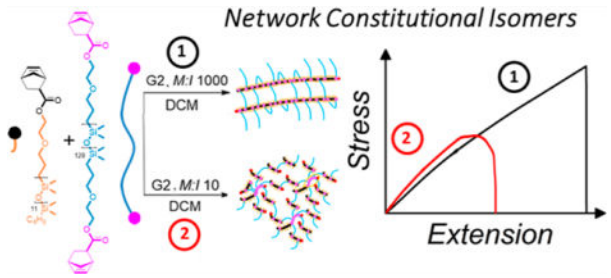

INTRODUCTION

Polymer networks are the fundamental building blocks for a wide variety of materials including tissue mimics, elastomers, and adhesives.[1–5] While a large range of architectural parameters have been varied to tune the mechanical properties of networks, the kinetic chain length (R_K) has been historically ignored. Indeed, from a physical standpoint, R_K has little

Corresponding Author: **Gregory N. Tew** – Department of Polymer Science and Engineering, University of Massachusetts Amherst, Amherst, Massachusetts 01003, United States; tew@mail.pse.umass.edu.

Complete contact information is available at: https://pubs.acs.org/10.1021/acs.macromol.3c01400

The authors declare no competing financial interest.

effect on the number of stress-supporting strands in models for modulus (affine, phantom, and RENT), apart from accounting for the dangling ends of some networks, or fracture.[6–11] Additionally, it is difficult to address the effects of R_K in networks specifically due to (1) the need for fine control over R_K and (2) chain entanglements confounding attempts to discern structure–property relationships.[12]

Fortunately, the easy-to-manipulate architecture of bottlebrush polymers and bottlebrush networks (BBNs) present an elegant solution to this problem.[13–15] BBNs are a class of polymer networks where the high grafting density and length of side chains stretch the polymeric backbone and its side-chains due to steric repulsion, leading to a marked lack of physical entanglements.[16–19] Polymerization of BBNs via a living polymerization method would provide direct control over R_K in a material in which the effects of entanglements can be disregarded. The highly popular ring-opening metathesis polymerization (ROMP) is uniquely positioned to study the role of R_K in BBNs due to its high conversion, living nature, lack of chain transfer, and established use in synthesizing BBNs.[9,20–23] Using ROMP, R_K can be easily controlled by varying the monomer-to-initiator ratio (M/I), with large M/Is producing longer R_Ks.

Herein, we synthesize BBNs via ROMP with M/Is ranging from 10 to 1000, generating R_Ks of 7.72 to 39.56 nm, respectively. These polymerizations were performed using Grubbs' second-generation catalyst (G2) because it is considered the most stable of the Grubbs' catalysts despite its tendency toward higher-molecular-weight dispersities.[24] The resulting BBNs display varied mechanical properties, including low frequency moduli, failure behavior, elongation at break, and adhesive strength. When macromonomer to cross-linker ratios are held constant, but the M/I ratio is varied, BBNs are formed with identical chemical compositions but varied chemical connectivity. Due to this unique attribute, we term them network constitutional isomers (NCIs—same chemical composition, same gel fraction, different connectivity) of one another. Given that they are constitutional isomers (identical elemental formula, different connectivity), the varied mechanical properties exhibited by NCIs *must* be due to the differences in their chemical connectivity, or network topology, controlled by R_K.

A molecular hypothesis for the formation and structure of these NCIs is proposed and supported by mechanical characterization data. This molecular hypothesis is rooted in an understanding of the relationship between the end-to-end distance of extended cross-links (R_{XL}), the R_K, and the mechanism of living polymerization. This understanding of NCI formation guided us to test a faster-initiating catalyst (Grubbs' third-generation). This catalyst produced NCIs with narrower R_K dispersities, generating shorter weight-average chains, resulting in fewer stress-supporting strands and therefore lower elastic modulus at the same cross-link density, or n_x (degree of polymerization between cross-links).[25] This increased understanding of constitutional isomerism demonstrates a new molecular approach to controlling network mechanical properties via only the slightest alterations in polymerization chemistry.

RESULTS AND DISCUSSION

NCI Design and Synthesis.

The BBNs within this study were synthesized via ROMP of PDMS macromonomers and bisnorbornyl PDMS cross-linkers (Figure 1). The degree of polymerization between cross-links (n_x) is controlled by varying the cross-link density (n_x^{-1} = 2× mol % cross-linker) to synthesize BBNs of varied material properties (e.g., elastic modulus). Of specific interest in this study is the effect of the R_K—an historically ignored variable within networks—on the mechanical properties of BBNs. Due to the living nature of ROMP and the absence of any significant chain transfer, the R_K of these ROMP polymers is controlled via variation of the M/I ratio. Within this study, M/I is varied from M/I = 10 to M/I = 1000 to synthesize BBNs with significantly different R_Ks. The gel fraction for all BBNs is >90% (Figure S5) and ssNMR confirms full conversion of closed-ring norbornene into open-ring norbornene (Figure 2), reiterating the high conversion of ROMP BBNs.[9]

Effect of R_K on Cross-Linker Consumption.

The relationship between R_K and cross-linker consumption is illuminated by examining the relative end-to-end distances of cross-linkers (R_{XL}) and R_K—see Supporting Information for details regarding modeling. The ratio of R_{XL}/R_K is used here to estimate what portion of the R_K contains cross-linkers that can still react with the living catalyst at the end of the chain (Figure 3). R_{XL} is represented by the radius of the dotted red circle around the catalyst at the end of each chain. Based on R_{XL}/R_K, the propagating catalyst at the ends of the M/I = 10 and M/I = 1000 chains are able to consume cross-links along the length of 75 and 15% of their R_K, respectively. This indicates that between the two systems, it is significantly more likely that the free end of a cross-link already incorporated into the backbone will be added to the end of the considerably shorter M/I = 10 chain. The shorter R_K chain will stop growing and remain the same size relative to extended cross-linkers after all macromonomer has been consumed. This will greatly increase the chances of intramolecular cyclization due to the living nature of ROMP. The dilute polymerization conditions further increase the likelihood of these intramolecular cyclizations.[26–28] In contrast, the longer R_K chain will be able to grow beyond this state, outpacing any dangling unconsumed cross-links due to physical separation of the catalyst from polymerizable moieties.

Effect of *M/I* on Cross-Linker Consumption.

Consider the case of two BBN polymerizations at reaction time t, with M/I = 10 and M/I = 1000 under otherwise identical polymerization conditions (Figure 4).[a] At a given time t, the M/I = 10 case has consumed 100% of the starting materials (macromonomer and cross-linker, see Figure 1). This is because the high initiator content (small M/I) grows many short chains—100 times more than in the M/I = 1000 case—which quickly polymerize all monomer and cross-linker in solution. Upon further reaction, the living chain ends (red circles) can only consume the remaining norbornenes of cross-linkers dangling from backbones, creating dense, consecutively cross-linked network junctions

[a]The M/I = 10 and M/I = 1000 samples were assigned DPs of 70 and 1840, respectively, based on light scattering (SEC MALS) of linear bottlebrush controls.

(pink circles) consisting of many cross-links but very few additional stress-supporting strands. In sharp contrast, at time t in the $M/I = 1000$ case, significantly more of the starting materials (macromonomer and cross-linker) remain in solution. The most likely reaction is further consumption of the starting monomers, allowing R_K to grow longer. This longer R_K increases the probability of adding effective cross-links along its length as the chain continues to grow (as described in Figure 3).

The overall effect of these varied additions is apparent in the final structures of the BBNs, where the distribution and chemical composition of cross-links throughout the two samples is markedly different (Figure 5). When these BBNs are synthesized with the same n_x, they are chemically identical but structurally dissimilar, making them NCIs of each other. We predicted that the varied distribution of cross-links and stress-supporting strands within these NCIs would manifest in different mechanical properties (e.g., elastic modulus, tensile behavior, and adhesion) derived from their topological connectivity.[8,29–31]

NCI Mechanics.

Based upon our understanding of the NCI structural details illustrated in Figure 5, it follows that $M/I = 10$ and $M/I = 1000$ NCIs should have varied numbers of stress-supporting strands due to differences in their molecular structures and cross-linker distributions. Due to the mechanism of the consecutive cross-linker phenomenon, it is likely that the addition of further cross-linker to the polymerization of the $M/I = 10$ BBNs would only result in a lengthening of the successive cross-linking at the end of the R_K, leading to no additional stress-supporting strands. In contrast, the $M/I = 1000$ NCIs are more likely to behave as expected ($E \propto n_x^{-1}$), with more stress-supporting strands being formed as n_x is lowered (recall that $n_x^{-1} \propto$ cross-link density).

Elastic Modulus.

To examine this hypothesis, a series of NCIs were synthesized at $M/I = 10$ and $M/I = 1000$ with n_x between 12.5 and 40.[9] Comparison of indentation results confirms that while the elastic modulus (E) scales with n_x for the $M/I = 1000$ NCIs, E for $M/I = 10$ NCIs are largely insensitive ($\parallel$) to changes in cross-link density (Figure 6a).[9] The limited influence of n_x on E further indicates that the number of stress-supporting strands within the $M/I = 10$ NCIs is constant within this range. The range of R_K where $E \parallel n_x$ was additionally investigated by synthesizing NCIs with intermediate M/Is between 10 and 1000 (Figure 6b). The observed $E \parallel n_x$ holds until $M/I = 500$, whereupon E begins to scale with n_x.

Networks at $M/I = 10$ and 1000 were produced with varied n_x values until E was identical between the two NCIs ($n_x = 40$). The equivalent values of E for these NCIs at $n_x = 40$ indicate that both have the same number density of stress-supporting strands despite the marked difference in their cross-link composition and distribution. These $n_x = 40$ samples represent a unique opportunity to determine the effects of constitutional isomerism on tensile behavior and adhesion, while holding the material's stiffness constant.

Tensile Testing.

Comparative tensile testing of these two NCIs with the same E (the n_x = 40 samples in Figure 6a) reveals that despite having the same cross-link density and E, their elongation at break (λ_{max}) and failure behaviors are quite different (Figure 7a). First, the λ_{max} of the M/I = 10 NCI is ~75% the value for the M/I = 1000 NCI. These differences in λ_{max} are a result of the more tightly cross-linked structure in the M/I = 10 NCI than the M/I = 1000 NCI. Second, while the M/I = 10 NCI fails at lower strain, its failure behavior displays a small plastic region (stress is independent of strain) prior to a slow decrease in stress with the increase in strain. This is strikingly different from the M/I = 1000 NCI which displays a more common pseudolinear increase in stress with applied strain before failure at a critical point.[23,32] This abrupt failure is typical of rapid crack propagation and unstable failure. Unlike the M/I = 1000 NCI, the toughened-like failure of M/I = 10 NCI is consistent with the molecular connectivity discussed previously in Figure 5. The densely connected cross-links formed in M/I = 10 NCI networks constitute one large, effective cross-link. As the applied strain increases, these sterically rigid network junctions undergo chain scission without reducing the overall number of local stress-supporting strands (Figure 7b). This is a known mechanism for toughening in networks as it provides a molecular mechanism for crack blunting to occur.[33,34] This blunting mechanism is severely limited in the M/I = 1000 NCIs, consistent with its observed critical stress failure.

Adhesion.

Tan(δ) provides a ratio of the viscous (nonstress-supporting strands) and elastic components of a network, where samples with more defects (network components not involved in stress-supporting strands) will exhibit larger tan(δ) values.[9,35] Comparison of the tan(δ) between the M/I = 10 and M/I = 1000 NCIs reveals that the M/I = 10 NCIs have nearly 2.5× lower tan(δ) than their isomeric counterparts (Figure 8a). This significantly lowered viscous contribution in the M/I = 10 NCI reflects the more interconnected structure of the network junction as opposed to the M/I = 1000 NCIs, which have dangling ends and longer stress-supporting strands with 10 kDa loop defects. The tan(δ) results are consistent with the proposed molecular network structures discussed earlier. In addition, the molecular network structures proposed would imply that for all M/I = 10 BBNs studied in Figure 6a, the tan(δ) data would be similar since they contain similar numbers of stress-supporting strands. Tan(δ) data for M/I = 10 BBNs with n_x = 40 and n_x = 12.5 show no significant differences in their viscous components as predicted (Figure 8a), even when the cross-link density is increased by a factor of ~3.2.

Tan(δ) experiments demonstrate NCIs provide an opportunity to hold the number of stress-supporting strands constant while altering the number of viscous, nonstress-supporting strands. This control over tan(δ) is particularly valuable for the design of materials with similar stiffness but different adhesive strengths.[5] Using the knowledge gleaned from the analysis of NCIs, a series of adhesive samples (n_x = 40) were synthesized and tested by hanging various weights from small sheets of Teflon held together by NCIs (Figure 8b). Due to their structural differences (small viscous components), M/I = 10 NCIs are less adhesive and only capable of lifting 50% as much weight as M/I = 1000 NCIs.

G2 and G3 NCIs.

Given our understanding of R_K's influence on the mechanical properties of NCIs, it follows that control over the dispersity of R_K will regulate the network properties. To examine this hypothesis, a series of NCIs were polymerized using Grubbs' third-generation catalyst (G3), which has a much faster initiation rate than the Grubbs' second-generation catalyst (G2) and should result in shorter R_Ks with narrower dispersities than those polymerized using G2.[25] Size-exclusion chromatography (SEC) and multiangle light scattering (MALS) of synthesized (M/I = 10) bottlebrush polymer controls (Figure 9b) confirm that the G3-initiated bottlebrushes are both shorter and less disperse than analogous G2 bottlebrushes.

The larger $Đ$ of G2-initiated polymerizations results in a population of chains with longer R_Ks. These longer chains have a greater probability of forming stress-supporting strands than the shorter chains of G3-initiated polymerizations. This population of chains is 1.6 times larger than those formed using G3 (Figure 9a), giving a smaller ratio of R_{XL}/R_K (49%). In contrast, the shorter R_K of the G3 samples (6.84 nm) results in a larger ratio of R_{XL}/R_K (85%), indicating that cross-links along 36% more of the G3 samples' R_K are within the range of the reactive chain end. This larger ratio results in *even fewer* stress-supporting strands being formed in the G3 NCIs. Indentation experiments reveal that G2 NCIs have E values ~1.7 times higher E than those of G3 NCIs (Figure 9c), confirming this hypothesis. The ability to control network properties by altering a single ligand (tricyclohexylphosphine or 2-bromopyridine) on the initiator further demonstrates the opportunities of this NCI design approach.

CONCLUSIONS

A series of NCIs was produced for the first time. Based on the living nature of ROMP, a molecular hypothesis was proposed to describe the structural differences between NCIs with varied R_K. NCIs produced with short R_Ks are shown to have E insensitive to cross-link density, reduced elongations-at-break, toughened failure behavior, and reduced viscous components compared to NCIs with longer R_Ks. These differences in the mechanical properties are consistent with the proposed molecular hypothesis. Using this understanding of R_K on network structure, a series of NCIs were produced using Grubbs' second- and third-generation catalysts (G2 and G3). The G3 NCIs had reduced E compared to G2 NCIs due to smaller weight-average molecular weight R_Ks. This investigation of constitutional isomerism in networks provides fundamentally new opportunities to control network mechanical properties via only minor alterations in polymerization chemistry.

EXPERIMENTAL SECTION

Synthesis of Monofunctional PDMS.

Norbornene-functionalized PDMS was synthesized via a Mitsunobu coupling reaction. Monobutyl PDMS (5.944 g, 5.40 mmol, Gelest) was placed in a dry round-bottom flask with a stir bar and dried overnight in a vacuum oven. The dried PDMS was dissolved in 30 mL of dried THF and placed under N_2 before adding *exo*-5-norbornene-2-carboxylic acid (1.490 g, 10.78 mmol, Sigma) and TPP (2.835 g, 10.81 mmol, Alfa Aesar) to the reaction mixture.

The stirring reaction mixture was chilled in ice water for 15 min before adding DIAD (2.120 mL, 10.77 mmol, Alfa Aesar) dropwise. The reaction was allowed to run 24 h before being concentrated, doused in hexanes, and refrigerated at −8 °C to precipitate triphenylphospine oxide (TPPO). The TPPO was removed using gravity filtration, and the resulting mixture was washed four times with methanol. The resulting mixture was concentrated and dried in a vacuum oven to remove excess hexanes. The product was a clear liquid, obtained at a yield of 86%. ^{1}H NMR (500 MHz, $CDCl_3$, δ): 6.09−5.99 (m, 2H), 4.21−4.10 (m, 4H), 3.60−3.50 (T, 2H), 3.40−3.32 (T, 2H), 3.00−2.95 (s, 1H), 2.91−2.82 (s, 1H), 2.23−2.15 (q, 1H), 1.90−1.80 (m, 1H), 1.60−1.44 (m, 4H), 1.35−1.15 (m, 7H), 0.03−(−)0.02 (m, 93.22H) (THF GPC in Figure S1, ^{1}H NMR in Figure S2).

Synthesis of Difunctional PDMS.

Norbornene-difunctionalized PDMS was synthesized via the Mitsunobu reaction in a manner identical to the monofunctional PDMS. To dried PDMS diol (5.023 g, 0.50 mmol, Gelest), *exo*-5-norbornene-2-carboxylic acid (0.278 g, 2.01 mmol, Sigma) and TPP (0.528 g, 2.01 mmol, Alfa Aesar) were added under N_2. DIAD (0.396 mL, 2.02 mmol, Alfa Aesar) was added dropwise to the reaction. The product was a clear, viscous liquid, obtained in a yield of 82%. ^{1}H NMR (500 MHz, $CDCl_3$, δ): 6.19−6.09 (m, 4H), 4.25−4.10 (t, 4H), 3.60−3.50 (T, 4H), 3.40−3.34 (T, 4H), 3.00−2.95 (s, 2H), 2.91−2.82 (s, 2H), 2.23−2.15 (q, 2H), 1.90−1.80 (m, 2H), 1.60−1.44 (m, 12H), 1.35−1.15 (m, 4H), 0.15−(−)0.15 (m, 985.02H) (THF GPC in Figure S1, ^{1}H NMR in Figure S3).

ROMP BBN Synthesis.

ROMP BBNs were synthesized by polymerizing norbornene-functionalized macromonomers (250 mg) with varied amounts of cross-linker. BBNs were all polymerized using either Grubbs' second-generation catalyst (Sigma) or Grubbs' third-generation catalyst at varied *M*/*I*s. For a typical reaction, the macromonomer and cross-linker were first dissolved in 1 mL of dried dichloromethane (DCM) in a 20 mL vial before adding 1 mL of catalyst/DCM solution. The reaction was allowed to run overnight before being quenched with three drops of ethyl vinyl ether (EVE, Sigma). Grubbs' third-generation catalyst was synthesized using 2-bromopyridine from published protocols.[36]

ROMP Bottlebrush Polymer Synthesis.

Bottlebrush polymerizations were performed in round-bottom flasks containing 20 mL of dried DCM with 125 mg of macromonomer and no cross-linker added to the reaction (Scheme S2). The synthesized bottlebrush polymers were characterized by SEC MALS and gel permeation chromatography (GPC) (Figure S4).

Nuclear Magnetic Resonance (^{1}H NMR, ^{13}C NMR, and ssNMR).

^{1}H NMR was used to determine the successful synthesis of macromonomer materials (Figures S2 and S3). ^{13}C NMR and ssNMR were used to determine the full conversion of closed-ring cross-linker norbornene to the open ring version seen in networks. NMR spectroscopy was performed by using a Bruker Advance 500 MHz NMR spectrometer with $CDCl_3$ as a solvent (when needed).

Gel Permeation Chromatography.

GPC was performed using an Agilent Technologies 1260 Infinity series system with two 5 μm mixed-D columns, a 5 μm guard column, a PL Gel 5 μm analytical Mixed-D column, and an RI detector (HP1047A); dried tetrahydrofuran (THF) was used as the eluent with a flow rate of 1.0 mL/min; polystyrene standards were used for the calibration. The dispersities ($Đ$) and molecular weights (M_w) of each macromonomer, cross-linker, and bottlebrush were measured using THF-GPC (Figures S1 and S4).

Size-Exclusion Chromatography Multi-Angle Light Scattering.

MALS was performed in THF +1 vol % triethylamine (TEA) using two Polymer Laboratories 10 μm mixed-B LS columns connected in series with a Wyatt Technologies DAWN EOS MALLS detector and RI detector at a flow rate of 1.0 mL/min. MALS was used to determine the M_w of synthesized bottlebrushes with an eluent of THF and 1% TEA.

Indentation and Tensile Testing with a Texture Analyzer.

Force/displacement data were collected by using a TA.XT Plus Texture Analyzer from Texture Technologies. Networks were indented with a 2 mm diameter probe at a loading rate of 0.01 mm/s to a force of 20 mN, whereupon the probe retracted at an unloading rate of 0.01 mm/s. The probe was cleaned with acetone between runs. Force/displacement data was analyzed using eq 1[37]

$$E = \frac{3}{8a}\frac{\Delta P}{\Delta \delta}\left\{1 + 1.33\frac{a}{h} + 1.33\left(\frac{a}{h}\right)^3\right\}^{-1} \quad (1)$$

where E is the elastic modulus, P is the load applied, a is the radius of the indentation probe, δ is the displacement of the probe, and h is the thickness of the sample. A Poisson's ratio of 0.5 is assumed for these calculations. Tensile testing was performed using tension clamps at a rate of 0.01 mm/s until tensile failure.

Dynamic Mechanical Analysis.

Networks were cut into 8 mm circles with a circular punch and placed within the compression clamps of a Discovery DMA 850 instrument from TA Instruments. Samples were tested at room temperature, sweeping in the frequency range 0.1–100 Hz at a strain amplitude of 1% with a preload force of 0.1 N. The sample stage was cleaned with isopropyl alcohol between samples. Refer to the Supporting Information for details regarding the adhesion tests.

Supplementary Material

Refer to Web version on PubMed Central for supplementary material.

ACKNOWLEDGMENTS

This research was funded by the U.S. Department of Education Graduate Assistance in Areas of Need (GAANN) Fellowship, the National Institute of Health (NIH) National Research Service Award T32 GM135096, and the Army Research Lab (ARL) Army Research Lab Award W911NF2120208. Facilities used during the conducting of this research are maintained by the University of Massachusetts, Amherst. Additional thanks are given to Dr. Weiguo Hu for assistance with solid state NMR.

REFERENCES

(1). Patrickios CS; Matyjaszewski K Amphiphilic Polymer Co-Networks: 32 Years Old and Growing Stronger - a Perspective. Polym. Int 2021, 70 (1), 10–13.

(2). Fan H; Gong JP Fabrication of Bioinspired Hydrogels: Challenges and Opportunities. Macromolecules 2020, 53 (8), 2769–2782.

(3). Sheiko SS; Dobrynin AV Architectural Code for Rubber Elasticity: From Supersoft to Superfirm Materials. Macromolecules 2019, 52 (20), 7531–7546.

(4). El-Atab N; Mishra RB; Al-Modaf F; Joharji L; Alsharif AA; Alamoudi H; Diaz M; Qaiser N; Hussain MM Soft Actuators for Soft Robotic Applications: A Review. Adv. Intell. Syst 2020, 2 (10), 2000128.

(5). Creton C; Ciccotti M Fracture and Adhesion of Soft Materials: A Review. Rep. Prog. Phys 2016, 79 (4), 046601. [PubMed: 27007412]

(6). Rubinstein M; Colby RH Polymer Physics, 2nd ed.; Oxford University Press: Oxford, NY, 2003.

(7). Akagi Y; Gong JP; Chung UI; Sakai T Transition between Phantom and Affine Network Model Observed in Polymer Gels with Controlled Network Structure. Macromolecules 2013, 46 (3), 1035–1040.

(8). Vatankhah-Varnosfaderani M; Daniel WFM; Everhart MH; Pandya AA; Liang H; Matyjaszewski K; Dobrynin AV; Sheiko SS Mimicking Biological Stress-Strain Behaviour with Synthetic Elastomers. Nature 2017, 549 (7673), 497–501. [PubMed: 28869962]

(9). Clarke BR; Kim H; Ilton M; Watkins JJ; Crosby AJ; Tew GN The Impact of Polymerization Chemistry on the Mechanical Properties of Poly(Dimethylsiloxane) Bottlebrush Elastomers. Macromolecules 2022, 55 (23), 10312–10319. [PubMed: 37502106]

(10). Zhong M; Wang R; Kawamoto K; Olsen BD; Johnson JA Quantifying the Impact of Molecular Defects on Polymer Network Elasticity. Science 2016, 353, 1264–1268. [PubMed: 27634530]

(11). Barney CW; Ye Z; Sacligil I; McLeod KR; Zhang H; Tew GN; Riggleman RA; Crosby AJ Fracture of Model End-Linked Networks. Proc. Natl. Acad. Sci. U.S.A 2022, 119, No. e2112389119.

(12). Lomellini P Effect of Chain Length on the Network Modulus and Entanglement. Polymer 1992, 33 (6), 1255–1260.

(13). Walsh DJ; Dutta S; Sing CE; Guironnet D Engineering of Molecular Geometry in Bottlebrush Polymers. Macromolecules 2019, 52 (13), 4847–4857.

(14). Yamauchi Y; Horimoto NN; Yamada K; Matsushita Y; Takeuchi M; Ishida Y Two-Step Divergent Synthesis of Monodisperse and Ultra-Long Bottlebrush Polymers from an Easily Purifiable ROMP Monomer. Angew. Chem. Int. Ed 2021, 60, 1528–1534.

(15). Choinopoulos I Grubbs' and Schrock's Catalysts, Ring Opening Metathesis Polymerization and Molecular Brushes-Synthesis, Characterization, Properties and Applications. Polymers 2019, 11, 298. [PubMed: 30960282]

(16). Paturej J; Sheiko SS; Panyukov S; Rubinstein M Molecular Structure of Bottlebrush Polymers in Melts. Sci. Adv 2016, 2 (11), No. e1601478.

(17). Xie G; Martinez MR; Olszewski M; Sheiko SS; Matyjaszewski K Molecular Bottlebrushes as Novel Materials. Biomacromolecules 2019, 20 (1), 27–54. [PubMed: 30296828]

(18). Daniel WFM; Burdyńska J; Vatankhah-Varnoosfaderani M; Matyjaszewski K; Paturej J; Rubinstein M; Dobrynin AV; Sheiko SS Solvent-Free, Supersoft and Superelastic Bottlebrush Melts and Networks. Nat. Mater 2016, 15, 183–189. [PubMed: 26618886]

(19). Kim H; Watkins JJ; Crosby AJ Adhesion and Mechanical Properties of Poly(Dimethyl Siloxane) Bottlebrush Elastomers. Soft Matter 2023, 19, 5311–5317. [PubMed: 37403551]

(20). Sarapas JM; Chan EP; Rettner EM; Beers KL Compressing and Swelling to Study the Structure of Extremely Soft Bottlebrush Networks Prepared by ROMP. Macromolecules 2018, 51 (6), 2359–2366.

(21). Clarke BR; Tew GN Synthesis and Characterization of Poly(Ethylene Glycol) Bottlebrush Networks via Ring-Opening Metathesis Polymerization. J. Polym. Sci 2022, 60, 1501–1510.

(22). Clarke BR; Tew GN Bottlebrush Amphiphilic Polymer Co-Networks. Macromolecules 2022, 55 (12), 5131–5139. [PubMed: 37485288]

(23). Cushman K; Keith A; Tanaka J; Sheiko SS; You W Investigating the Stress-Strain Behavior in Ring-Opening Metathesis Polymerization-Based Brush Elastomers. Macromolecules 2021, 54 (18), 8365–8371.

(24). Leitgeb A; Wappel J; Slugovc C The ROMP Toolbox Upgraded. Polymer 2010, 51 (14), 2927–2946.

(25). Walsh DJ; Lau SH; Hyatt MG; Guironnet D Kinetic Study of Living Ring-Opening Metathesis Polymerization with Third-Generation Grubbs Catalysts. J. Am. Chem. Soc 2017, 139 (39), 13644–13647. [PubMed: 28944665]

(26). Zhang K; Cui J; Lackey M; Tew GN Hydrogels Based on Living Ring-Opening Metathesis Polymerization. Macromolecules 2010, 43, 10246–10252.

(27). Madkour AE; Grolman JM; Tew GN Synthesis of Hydrogels via Ring-Opening Metathesis Polymerization: Factors Affecting Gelation. Polym. Chem 2011, 2 (1), 114–119.

(28). Tezuka Y; Komiya R Metathesis Polymer Cyclization with Telechelic Poly(THF) Having Allyl Groups. Macromolecules 2002, 35 (23), 8667–8669.

(29). Tian Y; Ina M; Cao Z; Sheiko SS; Dobrynin AV How to Measure Work of Adhesion and Surface Tension of Soft Polymeric Materials. Macromolecules 2018, 51 (11), 4059–4067.

(30). Daniel WFM; Burdyńska J; Vatankhah-Varnoosfaderani M; Matyjaszewski K; Paturej J; Rubinstein M; Dobrynin AV; Sheiko SS Solvent-Free, Supersoft and Superelastic Bottlebrush Melts and Networks. Nat. Mater 2016, 15 (2), 183–189. [PubMed: 26618886]

(31). Cao Z; Daniel WFM; Vatankhah-Varnosfaderani M; Sheiko SS; Dobrynin AV Dynamics of Bottlebrush Networks. Macromolecules 2016, 49 (20), 8009–8017.

(32). Vatankhah-Varnosfaderani M; Daniel WFM; Everhart MH; Pandya AA; Liang H; Matyjaszewski K; Dobrynin AV; Sheiko SS Mimicking Biological Stress-Strain Behaviour with Synthetic Elastomers. Nature 2017, 549 (7673), 497–501. [PubMed: 28869962]

(33). Luo F; Sun TL; Nakajima T; Kurokawa T; Zhao Y; Ihsan AB; Guo HL; Li XF; Gong JP Crack Blunting and Advancing Behaviors of Tough and Self-Healing Polyampholyte Hydrogel. Macromolecules 2014, 47, 6037.

(34). Wang Z; Zheng X; Ouchi T; Kouznetsova TB; Beech HK; Av-Ron S; Matsuda T; Bowser BH; Wang S; Johnson JA; Kalow JA; Olsen BD; Gong JP; Rubinstein M; Craig SL Toughening Hydrogels through Force-Triggered Chemical Reactions That Lengthen Polymer Strands. Science 2021, 374 (6564), 193–196. [PubMed: 34618576]

(35). Muthukumar M Screening Effect on Viscoelasticity near the Gel Point. Macromolecules 1989, 22, 4656–4658.

(36). Love JA; Morgan JP; Trnka TM; Grubbs RH A Practical and Highly Active Ruthenium-Based Catalyst That Effects the Cross Metathesis of Acrylonitrile. Angew. Chem., Int. Ed 2002, 41 (21), 4035–4037.

(37). Shull KR; Ahn D; Chen W-L; Flanigan CM; Crosby AJ Axisymmetric Adhesion Tests of Soft Materials. Macromol. Chem. Phys 1998, 199 (4), 489–511.

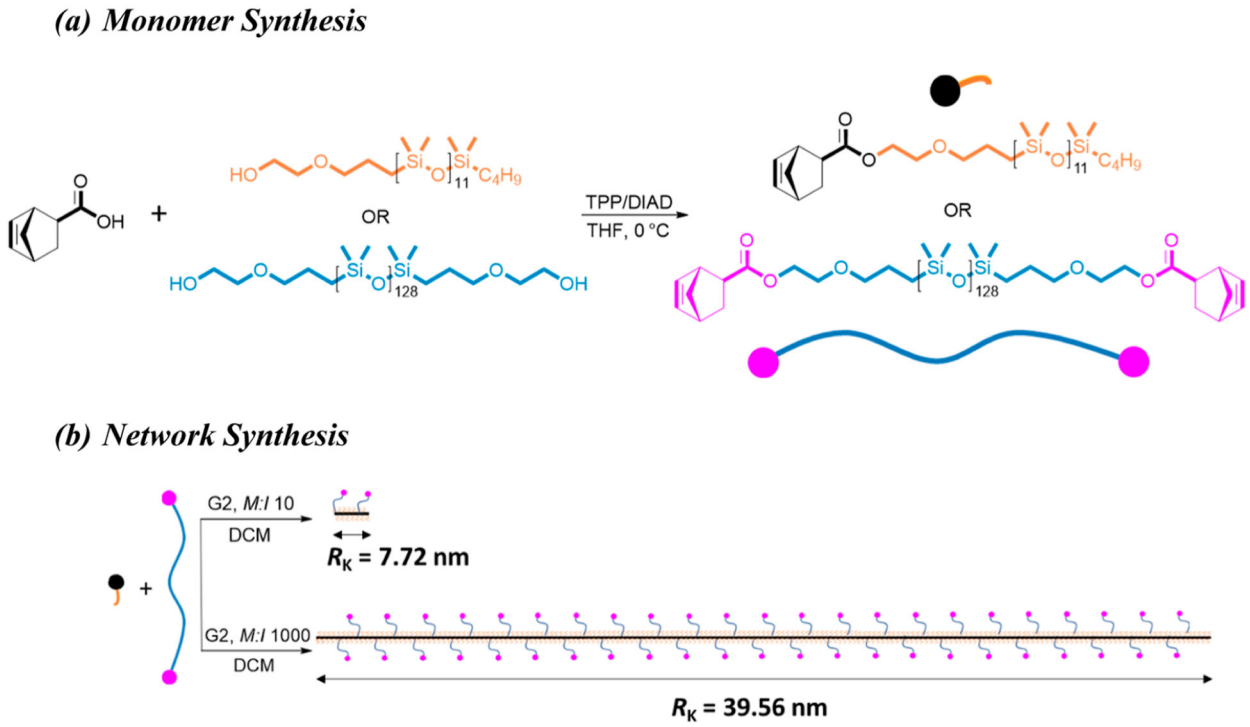

Figure 1.

(a) Synthesis of the norbornene-functionalized PDMS macromonomer and cross-linker via the Mitsunobu reaction. The macromonomer and cross-linker will henceforth be represented as a black monomer-head with an orange chain and a pink monomer-head with a blue chain, respectively. (b) Synthesis of NCIs with kinetic chain length (R_K) controlled by M/I (M here refers to the macromonomer content only, not considering the cross-linker content). The black backbones represent R_K values for each network. A cross-link density of $n_x = 40$ (1.2 mol %) is illustrated by the spacing between cross-links attached along R_K (loops or other defects are not shown for clarity). The ends of cross-links (pink heads) are depicted as unconsumed only for the sake of clarity regarding R_K, actual samples have no unconsumed cross-links (see Figure 2). Note that n_x is an average of the DP between cross-links in networks; real networks have a distribution of cross-link lengths.

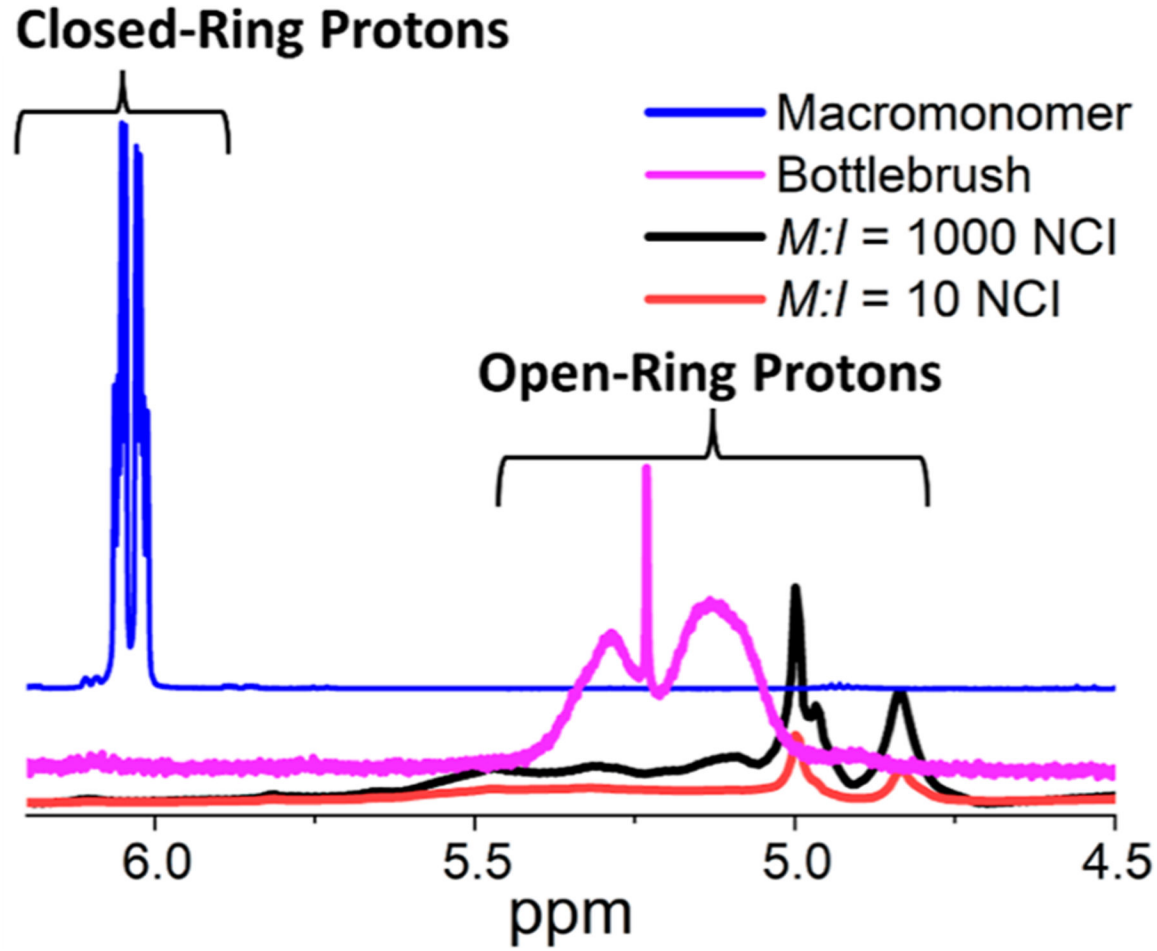

Figure 2.

Solid and solution state ^{1}H NMR detailing the conversion of closed-ring macromonomer protons to the open-ring protons of the polymerized bottlebrushes and NCIs. Note that both NCIs have no remaining macromonomer proton signals. The NCIs chosen for this study were n_x = 12.5, the highest cross-link density samples of those investigated during this study. As all closed-ring signals have disappeared in these highly cross-linked samples, we conclude that all the more lightly cross-linked samples studied herein have also reached full conversion (supported by their high gel fractions—greater than 90%). For comparison, we have also included the solution-state ^{1}H NMR for a poly(norbornene)-*g*-poly-(dimethylsiloxane) bottlebrush polymer (pink), composed of entirely macromonomer with no cross-linker added to the polymerization.

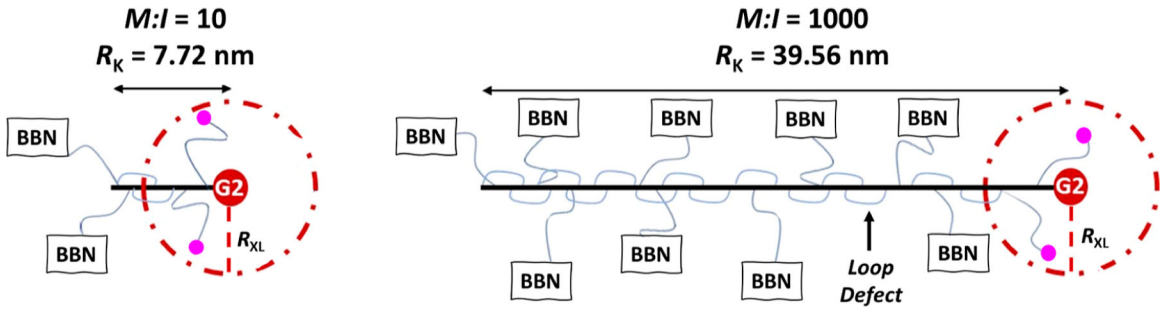

Figure 3.

Graphical depiction of the differences in R_K between synthesized $M/I = 10$ and $M/I = 1000$ NCIs (lengths as determined via SEC MALS) [side chains have been removed for clarity]. The red dotted circles surrounding the living catalysts at the chain end represent the area (volume) within which a cross-link can still be added to the end of a growing chain. For the 7.72 nm chain ($M/I = 10$), cross-links along ~75% of the chain are within this circle and can be added to the end of the chain. In contrast, the cross-links of the 39.56 nm chain ($M/I = 1000$) can only be added along ~15% of the R_K, allowing stress-supporting strands to be formed more effectively. This reduced distance (15 vs 75%) allows more cross-links to remain available for network formation. Refer to the Supporting Information for details regarding these calculations.

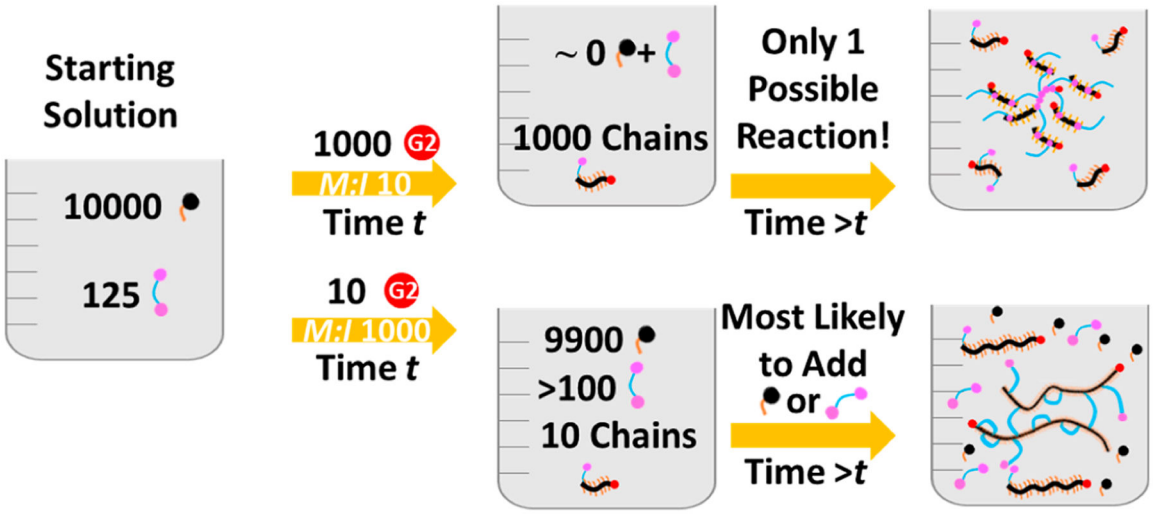

Figure 4.

Conceptual schematic illustrating how differences in catalyst amounts result in altered cross-link distributions despite identical starting materials. The number of chains in solution is directly proportional to the amount of the catalyst added to the reaction. The larger number of propagating chains in the (top) *M*/*I* 10 polymerization results in all monomers and cross-linkers in solution being consumed relatively early (time *t*). The living nature of the catalyst and the large number of chains in solution will eventually (time > *t*) add any unconsumed cross-links hanging from already polymerized chains. This effect will repeat until either the catalyst dies or all remaining cross-links are consecutively consumed. The smaller number of chains in the (bottom) *M*/*I* 1000 polymerization—100 times fewer—results in many monomers and cross-linkers remaining at the same point in the *M*/*I* 10 polymerization (time *t*). As the polymerization continues (time > *t*) the propagating chains are significantly most likely to add new monomers or cross-linkers to the growing chain-end. This results in a more statistical distribution of cross-links, with the consecutive cross-linking effect observed in the *M*/*I* 10 case being severely curtailed by the small quantity of active catalyst in solution.

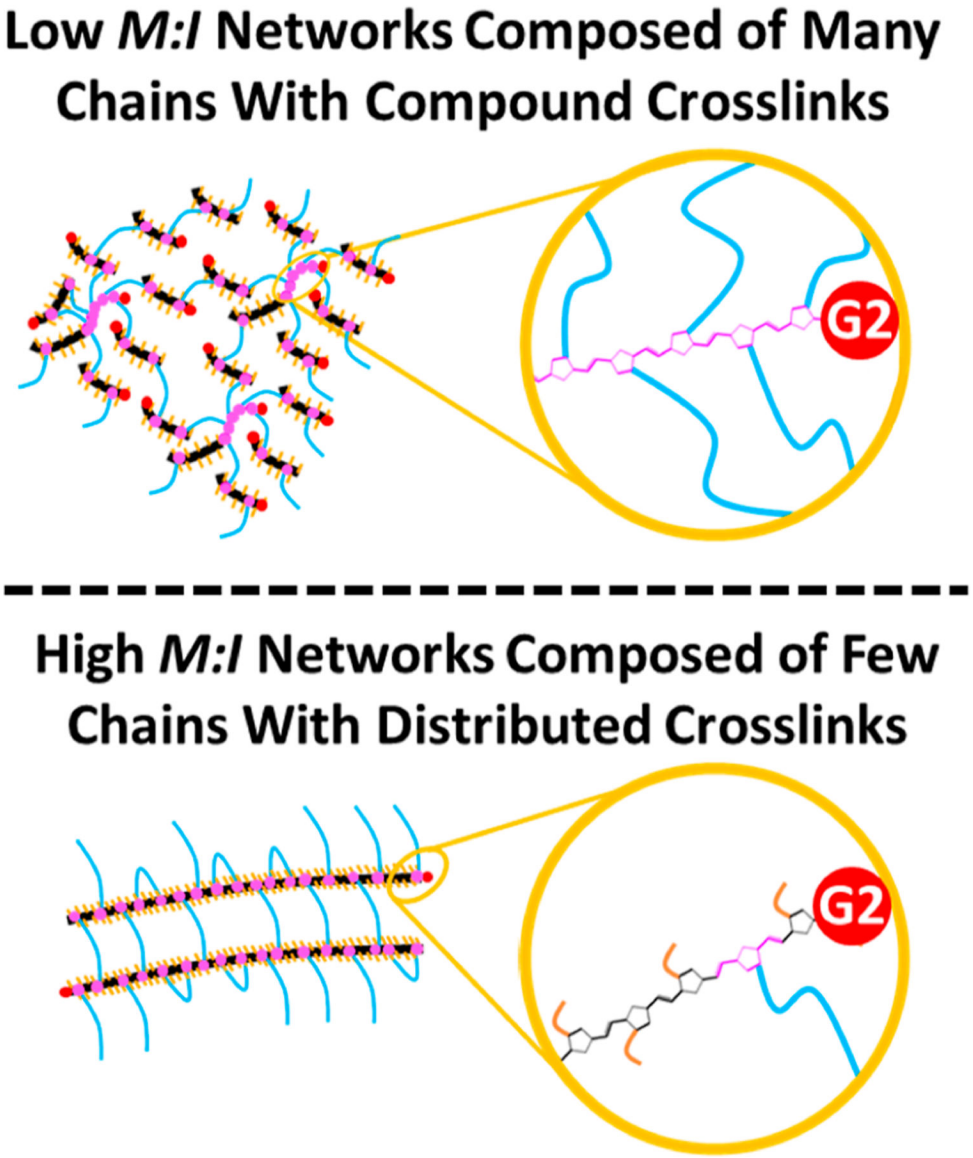

Figure 5.

Schematic illustrations of (top) low M/I networks containing many small chains and compound cross-links and (bottom) high M/I networks with only a few, large chains containing statistical distributions of cross-links. The transition between the two "regimes" occurs somewhere between M/I = 250 and 500 (Figure 6b).

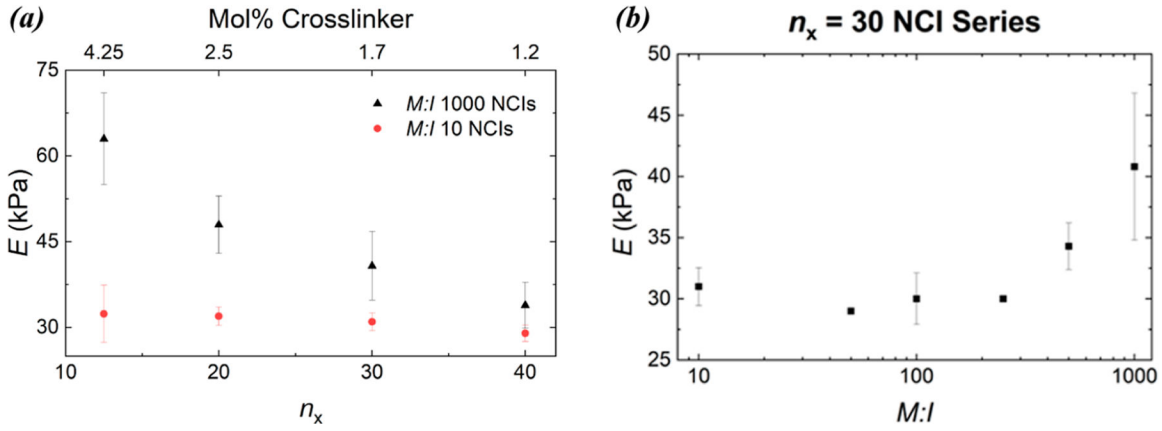

Figure 6.

(a) Elastic modulus (E) plotted as a function of n_x for a range of M/I = 10 and 1000 NCIs. The E values here were determined through indentation (Figure S7) of several samples with a disc geometry using a flat punch probe at a strain rate of 10 μm/s. Of special interest is how the E of M/I = 10 NCIs does not scale as expected with n_x ($E \propto n_x^{-1}$), while the M/I = 1000 NCIs display the expected increase in E as n_x decreases. These data are consistent with the network structures introduced in Figure 4, where additional cross-linking in M/I = 10 NCIs produces no new stress-supporting strands. Note: above n_x = 40 for M/I = 10, networks are no longer made since n_x begins to approach the degree of polymerization for R_K (DP = 70). (b) Plot of E illustrating how this effect persists until the M/I of the polymerization is increased to 500.

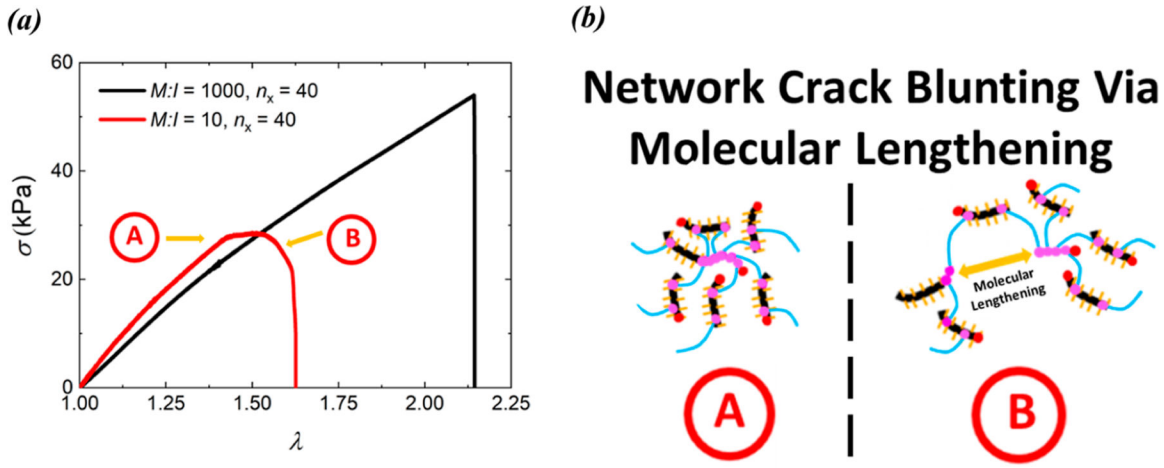

Figure 7.

(a) Tensile testing of M/I = 10 and 1000 NCIs with n_x = 40. Despite having similar E values (see Figure 6), the NCIs have different elongations at break and failure behaviors. The M/I = 10 NCI shows failure uncommon to PDMS BBNs, while the M/I = 1000 NCI fails as expected (λ = [strain + original sample length]/original sample length). (b) Schematic illustration of the consecutive cross-link in an M/I = 10 NCI. As tensile elongation begins to break bonds within the NCI, chain scission at the sterically primed compound cross-links dissipates force, providing a molecular mechanism for local stress relaxation and crack-blunting.[34]

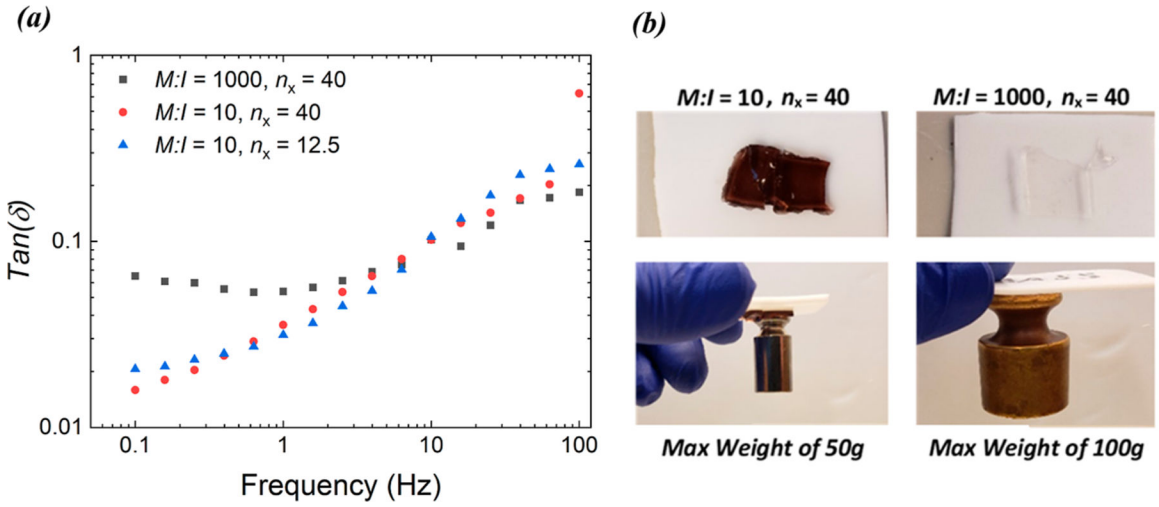

Figure 8.

(a) Plot of the loss tangents [tan(δ)] of three BBNs, determined from dynamic mechanical analysis. For M/I = 10 and M/I = 1000 NCI—even with the same n_x (40) and E—these NCIs have very different low frequency loss tangents. For M/I = 10 at n_x = 40 and 12.5, their E and tan(δ) values are identical despite having different cross-link densities (3.2×). The tan(δ) data are consistent with the network structures proposed in Figure 4. The M/I = 1000 NCIs have many more loss-contributing defects than the M/I = 10 NCIs (at the same n_x). Similarly, the M/I = 10 BBNs have the same E regardless of n_x consistent with the same density of cross-links (or stress-supporting strands). (b) The larger viscous component of the M/I = 1000 NCIs makes it a stronger pressure-sensitive adhesive than the M/I = 10 NCIs, enabling the carrying of twice the mass when adhered to sheets of Teflon. For reference, the surface areas of the weight tops are ~2.00 and 3.14 mm^2 for the 50 and 100 g weights, respectively.

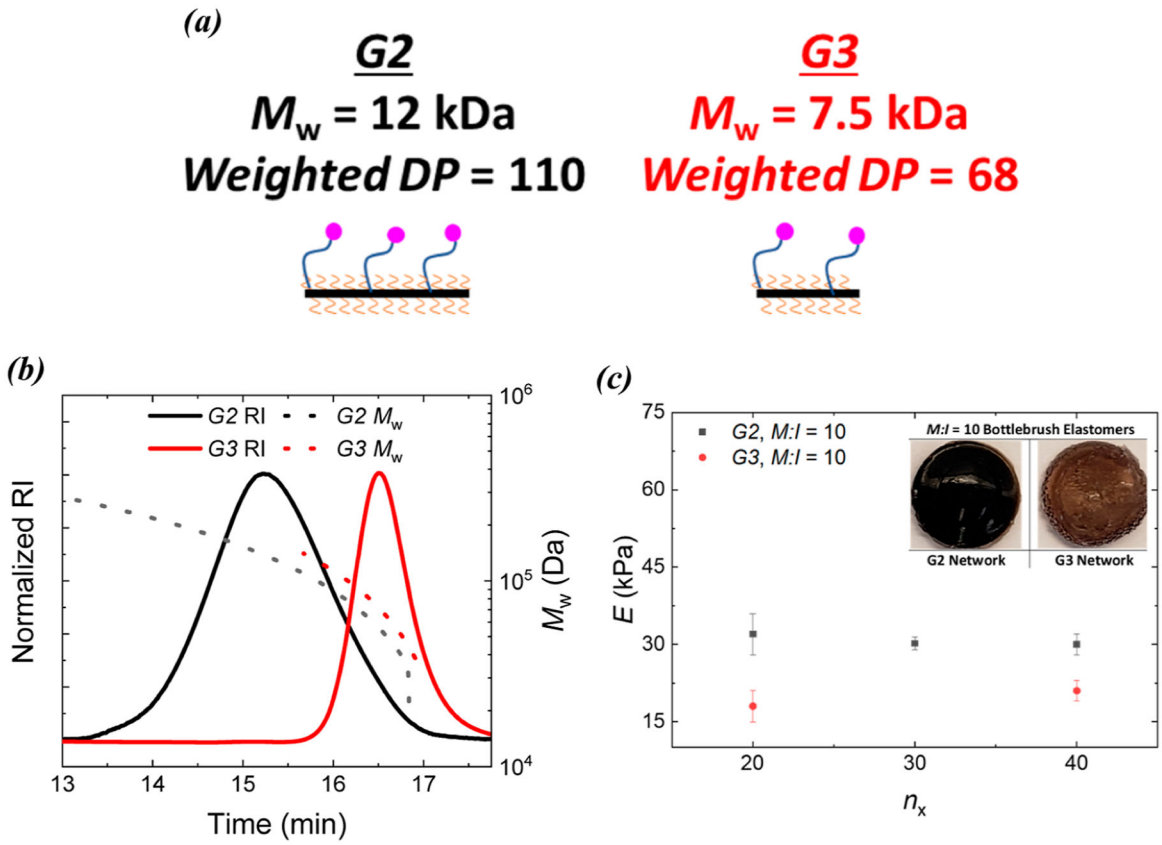

Figure 9.

(a) Impact on R_K of using G2 or G3 to polymerize $M/I = 10$ BBNs. Both generate R_Ks larger than the M/I ratio but G2 provides a larger dispersity of molecular weights, weighted with longer R_Ks. The weight-average molecular weights are 12 and 7.5 kDa for G2 and G3, respectively (corresponding to weighted DPs of 110 and 68). The impact of these weight-average molecular weights on R_K and average number of cross-links per chain are illustrated schematically. (b) SEC MALS of linear bottlebrush controls synthesized using either G2 (black) or G3 (red) catalysts at $M/I = 10$ in the absence of a cross-linker. The solid and dashed curves correspond to the refractive index (RI) and light-scattering data collected via SEC MALS respectively. MALS data illustrate that the G2 sample contains a population of chains that are longer than the G3 sample due to the higher dispersity associated with G2. Data from all bottlebrush controls are compiled in Table S2. (c) Elastic modulus (E) vs n_x for $M/I = 10$ NCIs synthesized using G2 and G3 catalysts. The G3 NCIs have lower E values than analogous G2 NCIs due to their shorter R_Ks. The inset contains photos of the $n_x = 40$ NCIs described in the plot. The $M/I = 10$ NCIs are dark in color due to the presence of 10^2 more ruthenium catalyst than the $M/I = 1000$ BBNs.